Supporting Information

Construction of Reversible-cycling Bifunctional Electrocatalyst $CoP_2@Co(CO_3)_{0.5}OH/Cu/NF$ with Mott-Schottky structure for Overall Water Splitting

Xinyuan Liao [a†], Xiaomin Lang [a†], Ting Zhang [a], Chunmei Li [a], Jian Zou [c], Qing Li [a], Weihua Hu [a], and Hua Lin [a,b] *

a. School of Materials and Energy, Southwest University, Chongqing 400715, P. R. China.

b. Yibin Academy of Southwest University, Yibin, 64400, P. R. China.

c. School of Chemistry and Chemical Engineering, Southwest University, Chongqing 400715, P. R. China.

† These authors contributed equally to this work.

*Corresponding author: lh2004@swu.edu.cn

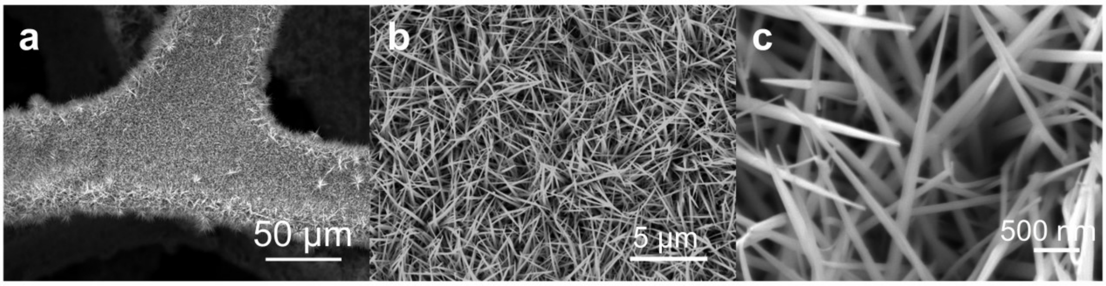

Figure S1. (a-c) The SEM images of $Co(CO_3)_{0.5}OH$/Cu/NF at different magnifications (Corresponding to the magnification of CoP_2@$Co(CO_3)_{0.5}OH$/Cu/NF).

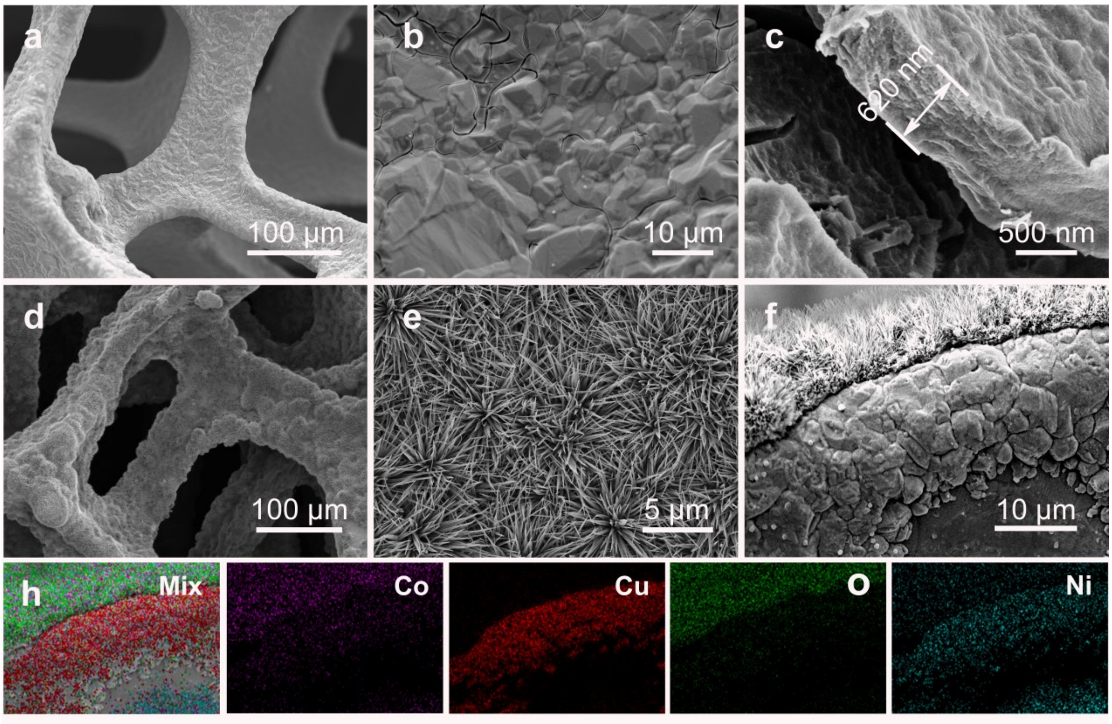

Figure S2. (a-b) SEM images of Cu/NF; (c) Thickness of the copper layer on the surface of Cu/NF; SEM images of $Co(CO_3)_{0.5}OH$/Cu/NF (d-e) and $Co(CO_3)_{0.5}OH$/Cu/NF surface etching sites, and the corresponding EDS plots (f-h).

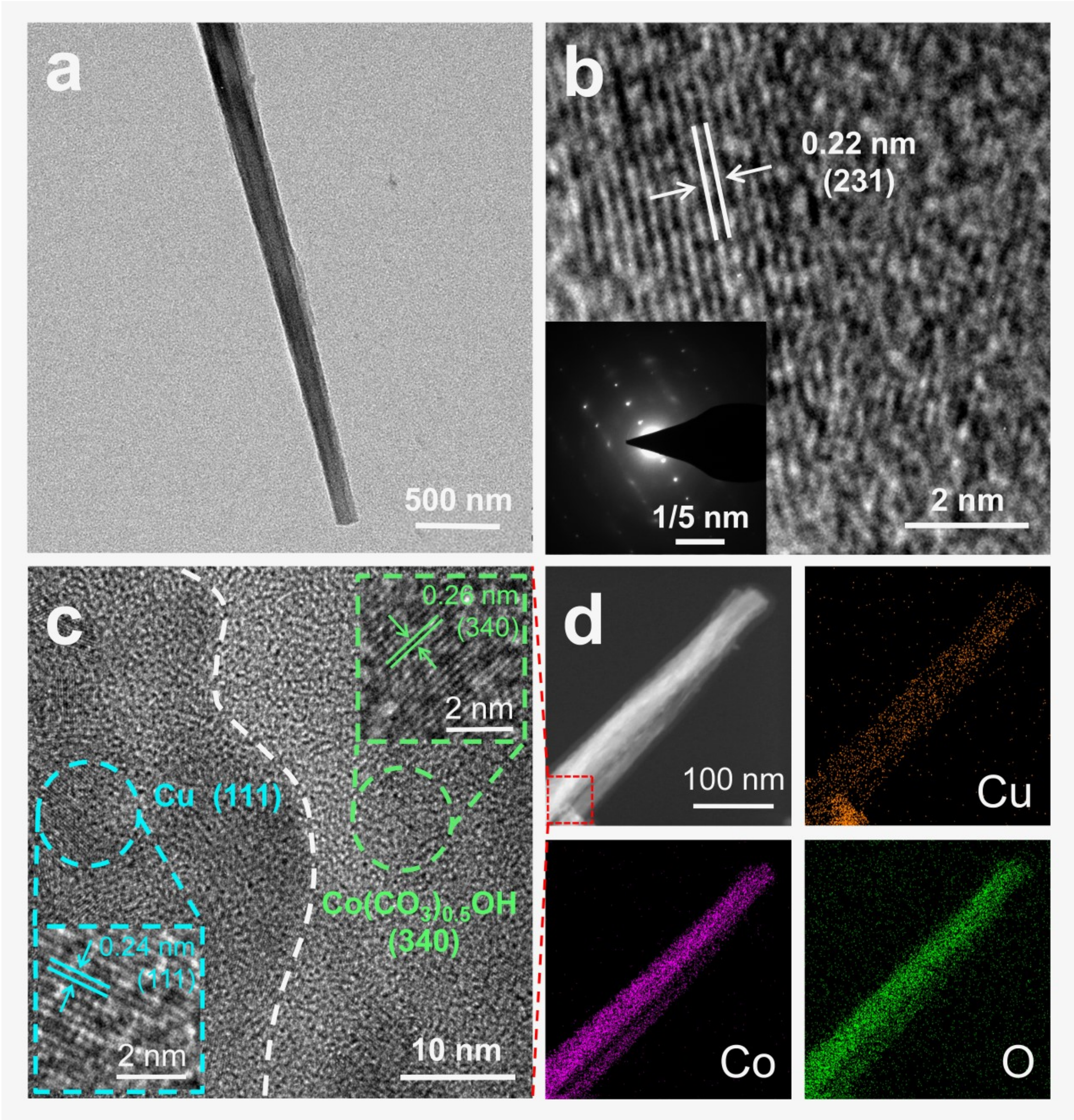

Figure S3. (a) TEM image of $Co(CO_3)_{0.5}OH$ nanowire; (b) HRTEM image of $Co(CO_3)_{0.5}OH$ nanowire (The inset is an electron diffraction pattern); (c) HRTEM image; (d) Distribution of elements at $Co(CO_3)_{0.5}OH$ and Cu heterojunctions.

As shown in Fig.S3a, $Co(CO_3)_{0.5}OH$ nanowires can be more clearly observed in the transmission electron microscope of $Co(CO_3)_{0.5}OH$ /Cu/NF. As shown in Figure 3b, the lattice spacing on the nanowire substrate is d ≈ 0.22 nm, corresponding to the (231) crystal plane of $Co(CO_3)_{0.5}OH$. The selected area electron diffraction (SAED) pattern shows a regular lattice, indicating that the nanowires have good crystallinity. Then the high-resolution TEM analysis is carried out. In Figure 3c, the white dotted line is used as the interface. The d≈0.24 nm of the left lattice fringe corresponds to the (111) crystal plane of Cu, while the d≈0.22 nm of the region on the right side of the white dotted line corresponds to the (231) crystal plane of $Co(CO_3)_{0.5}OH$. The left and right sides of the imaginary line correspond to the metal Cu phase and $Co(CO_3)_{0.5}OH$ phase, respectively, indicating that a heterojunction structure is formed between Cu and $Co(CO_3)_{0.5}OH$ phases. The energy dispersive X-ray (EDX) element mapping of Figure S3d shows that the Co and O signals are uniformly distributed on the nanowires, while the Cu signal is concentrated on the nanosheets in the lower left corner, which is consistent with the formation of Cu and $Co(CO_3)_{0.5}OH$ heterojunction.

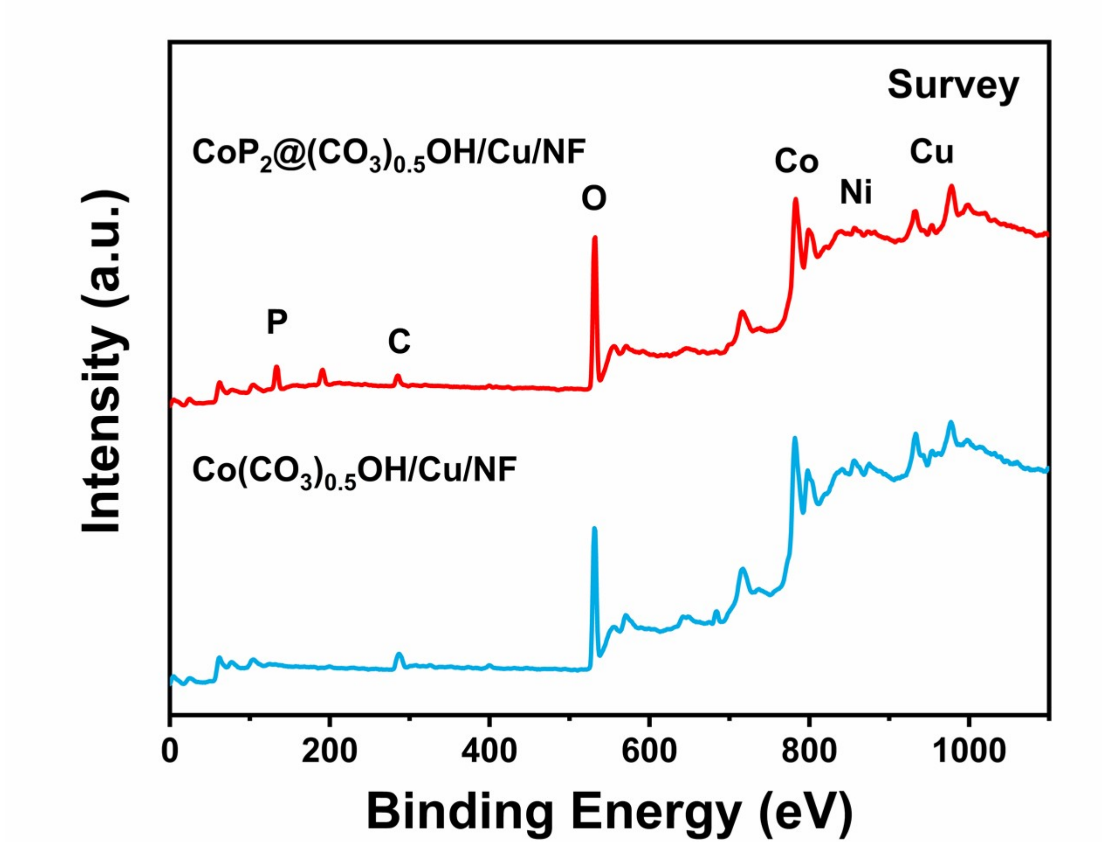

Figure S4. Total XPS spectrum of $CoP_2@Co(CO_3)_{0.5}OH/Cu/NF$ and $Co(CO_3)_{0.5}OH/Cu/NF$.

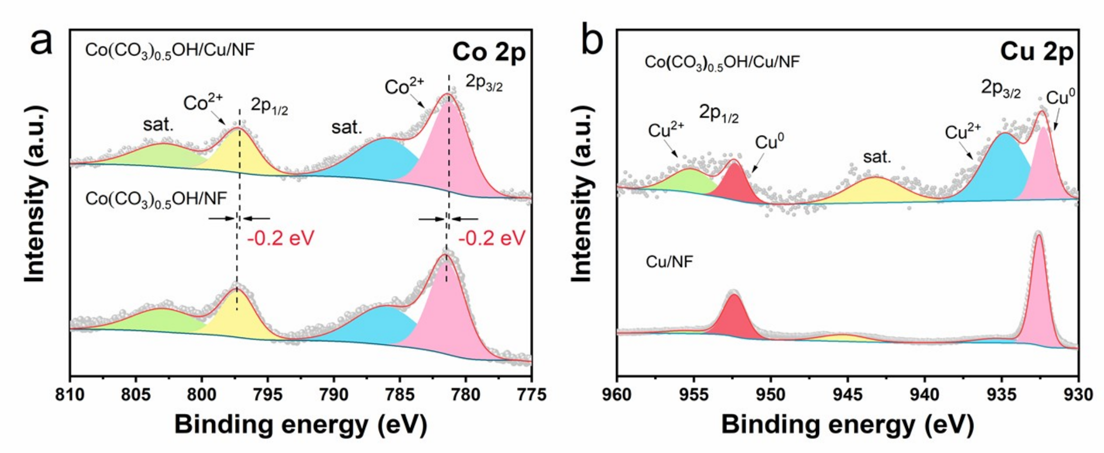

Figure S5. XPS spectra of $Co(CO_3)_{0.5}OH$ /Cu/NF (a)Co 2p; (b)Cu 2p.

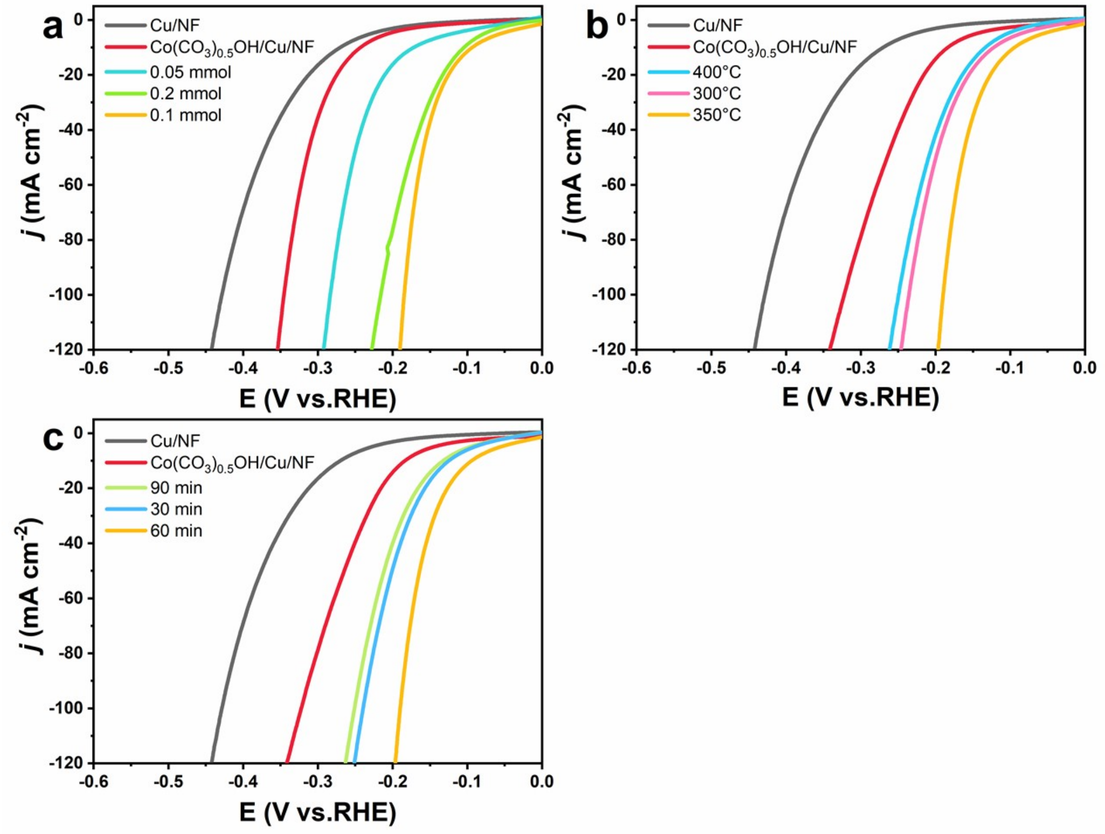

Figure S6. Effect of different conditions on HER activity (a) Molar mass of sodium hypophosphite; (b) Phosphating temperatures; (c) Phosphating time.

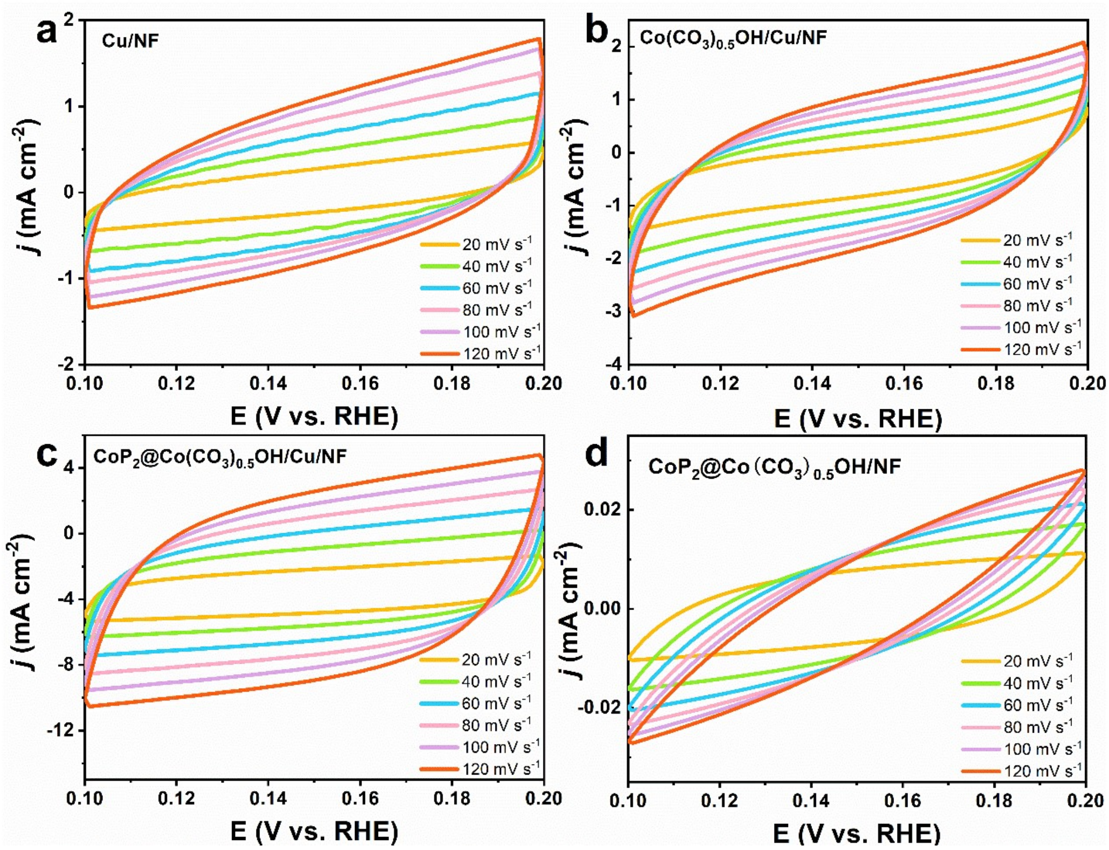

Figure S7. CV curves in the region of 0.2-0.3 V for (a) Cu/NF, (b) $Co(CO_3)_{0.5}OH$/Cu/NF, (c) CoP_2@$Co(CO_3)_{0.5}OH$/Cu/NF and (d) CoP_2@$Co(CO_3)_{0.5}OH$/NF at various scan rates. (20, 40, 60, 80, 100, and 120 mV s^{-1}).

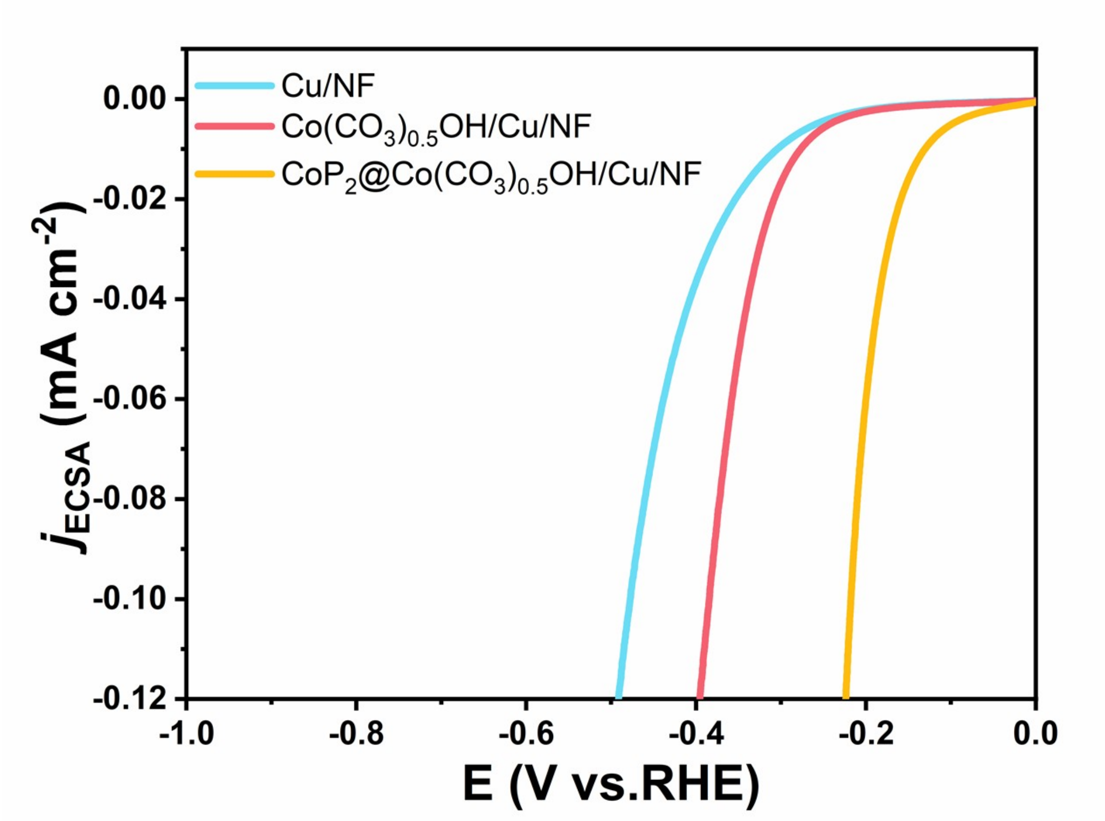

Figure S8. ECSA-normalized LSV curves of Cu/NF, $Co(CO_3)_{0.5}OH/Cu/NF$, and $CoP_2@Co(CO_3)_{0.5}OH/Cu/NF$ in HER. (The Cdl is converted to ECSA using the specific capacitance value for a flat surface of 0.04 mF cm^{-2}).

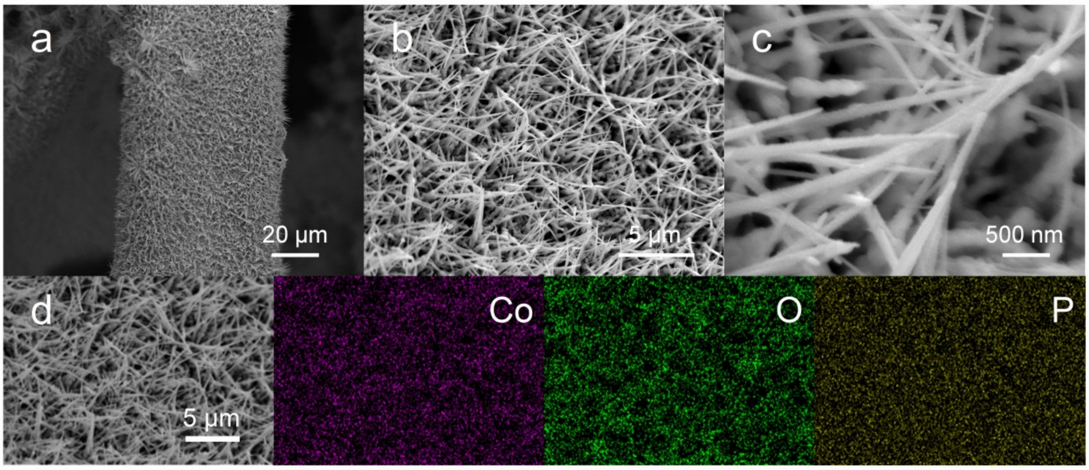

Figure S9. The SEM images of $CoP_2@Co(CO_3)_{0.5}OH/Cu/NF$ after HER

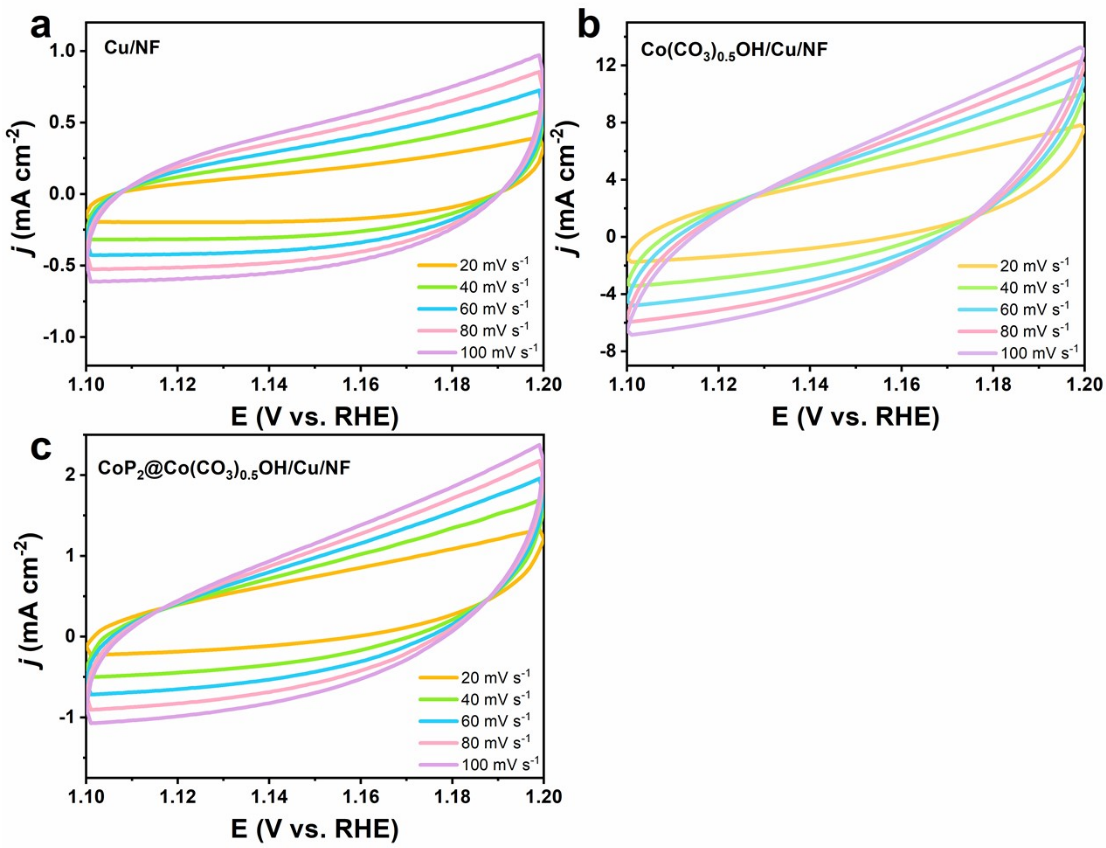

Figure S10. CV curves in the region of 1.13-1.23 V for (a) Cu/NF, (b) $Co(CO_3)_{0.5}OH$/Cu/NF, and (c) CoP_2@$Co(CO_3)_{0.5}OH$/Cu/NF at various scan rates. (20, 40, 60, 80, and 100 mV s^{-1}).

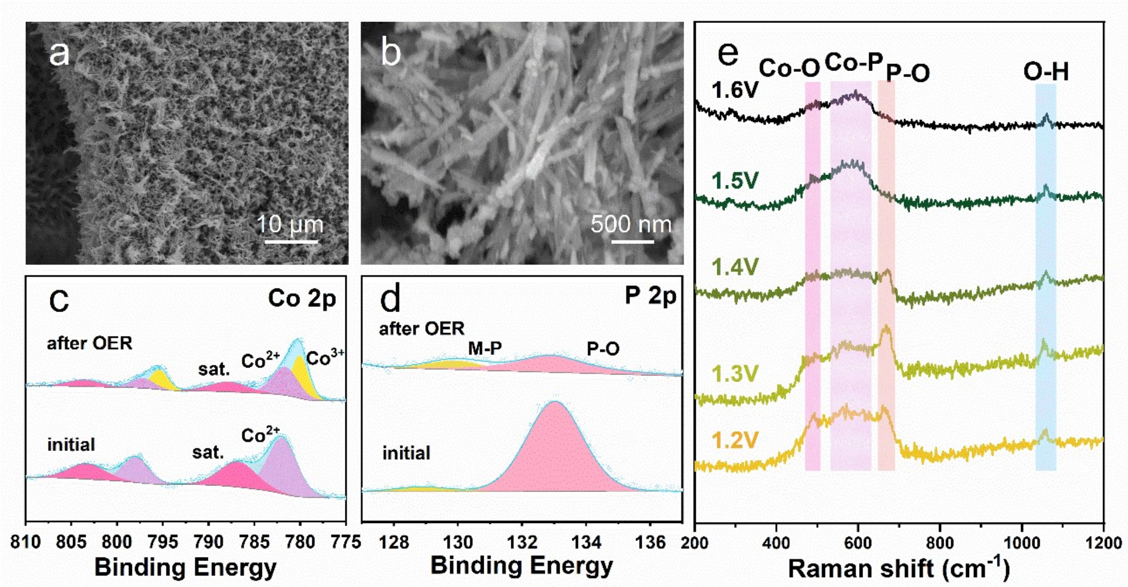

Figure S11. (a-b) SEM images and (c-d) XPS spectra of $CoP_2@Co(CO_3)_{0.5}OH/Cu/NF$ after the OER, (e) In-situ Raman pattern of the sample during OER process.

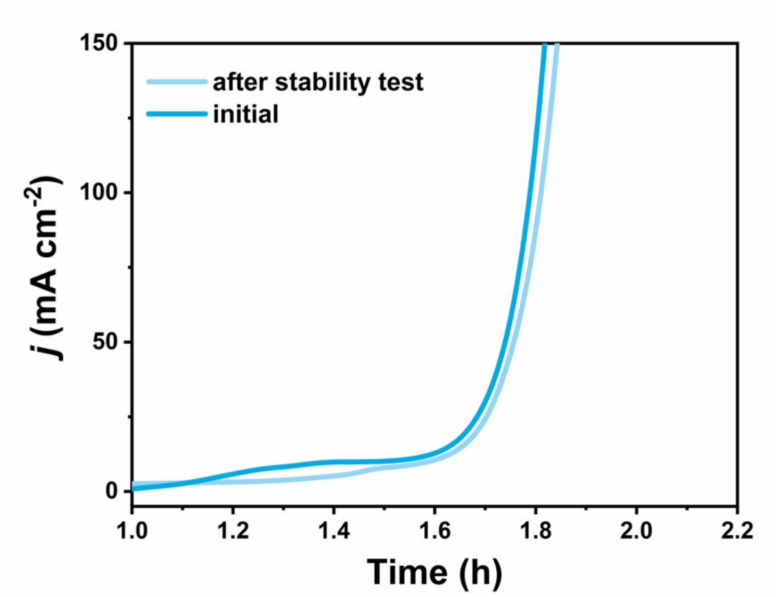

Figure S12. The overall water splitting properties of $CoP_2@Co(CO_3)_{0.5}OH/Cu/NF$ (+, -) before and after 48 h.

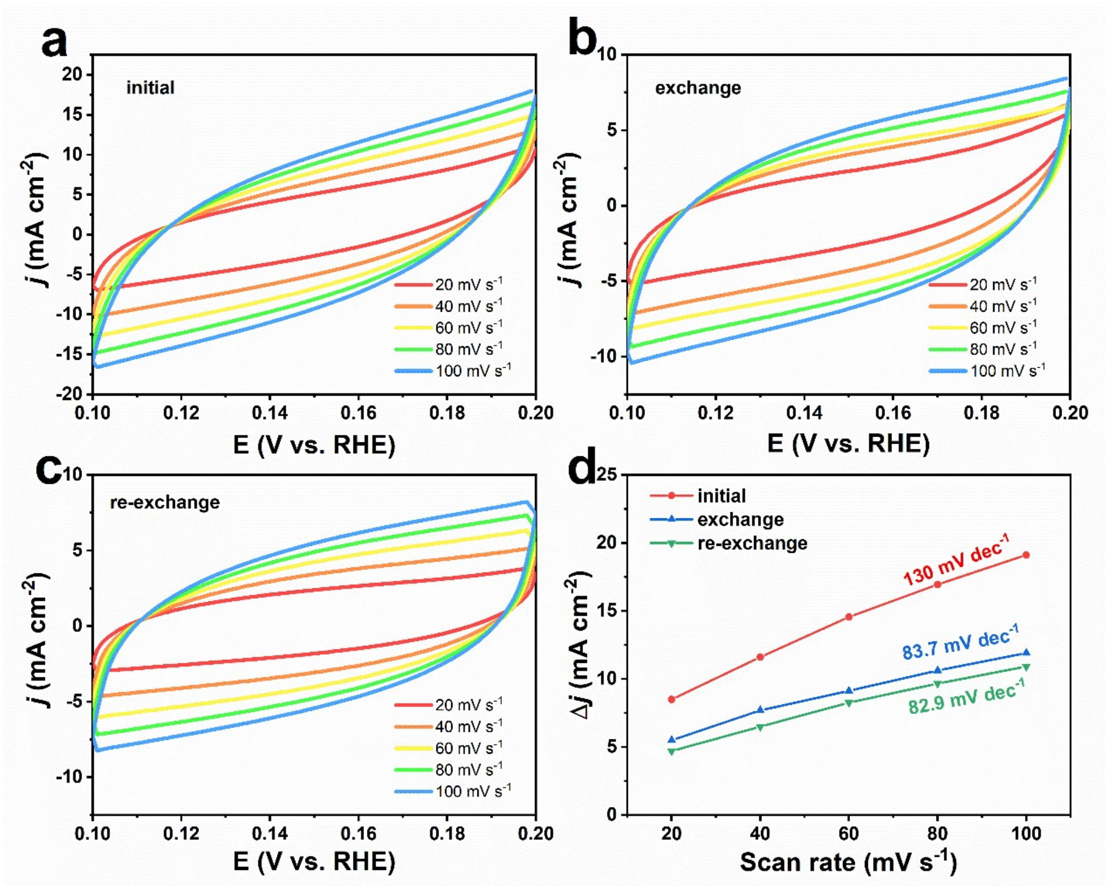

Figure S13. (a-c) CV curves of the initial anode, after exchange, and re-exchange; (d) C_{dl} values of the above samples (test voltage range is 0.1-0.2 vs RHE).

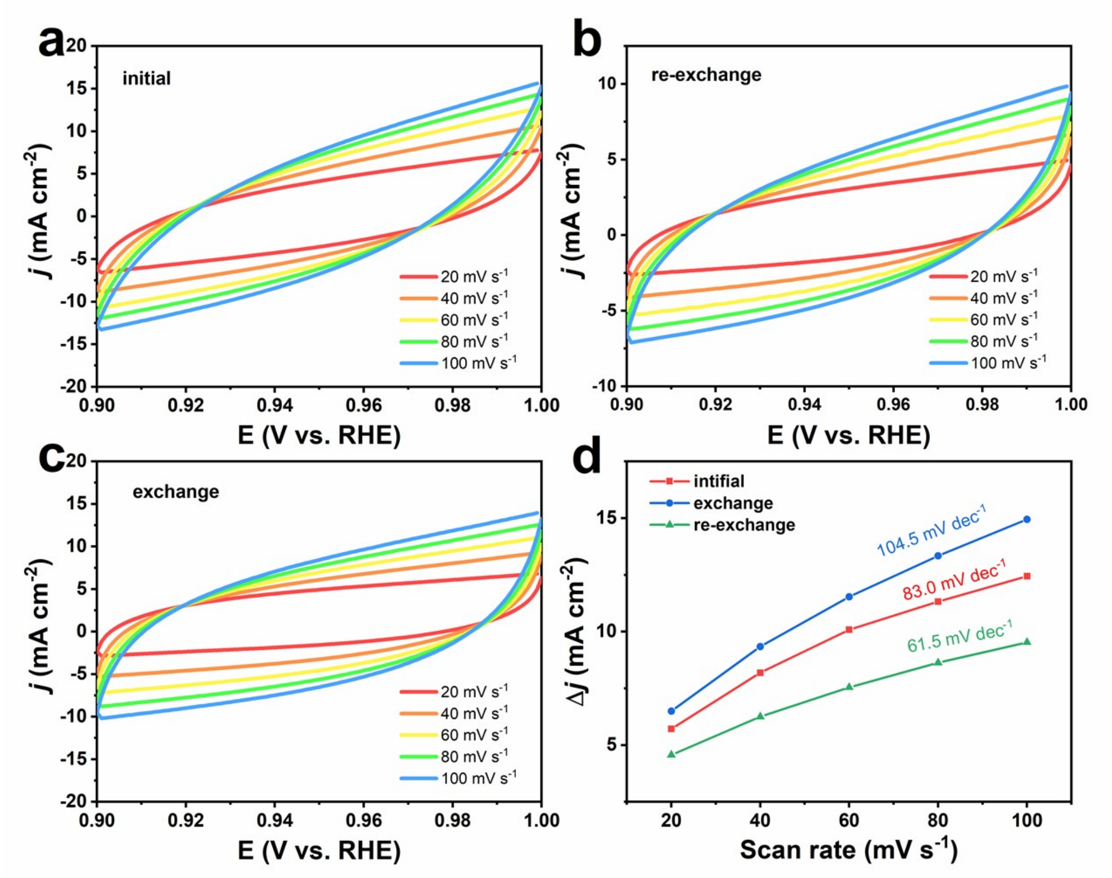

Figure S14. (a-c) CV curves of the initial anode, after exchange, and re-exchange; (d) C_{dl} values of the above samples (test voltage range is 0.9-1.0 vs RHE).

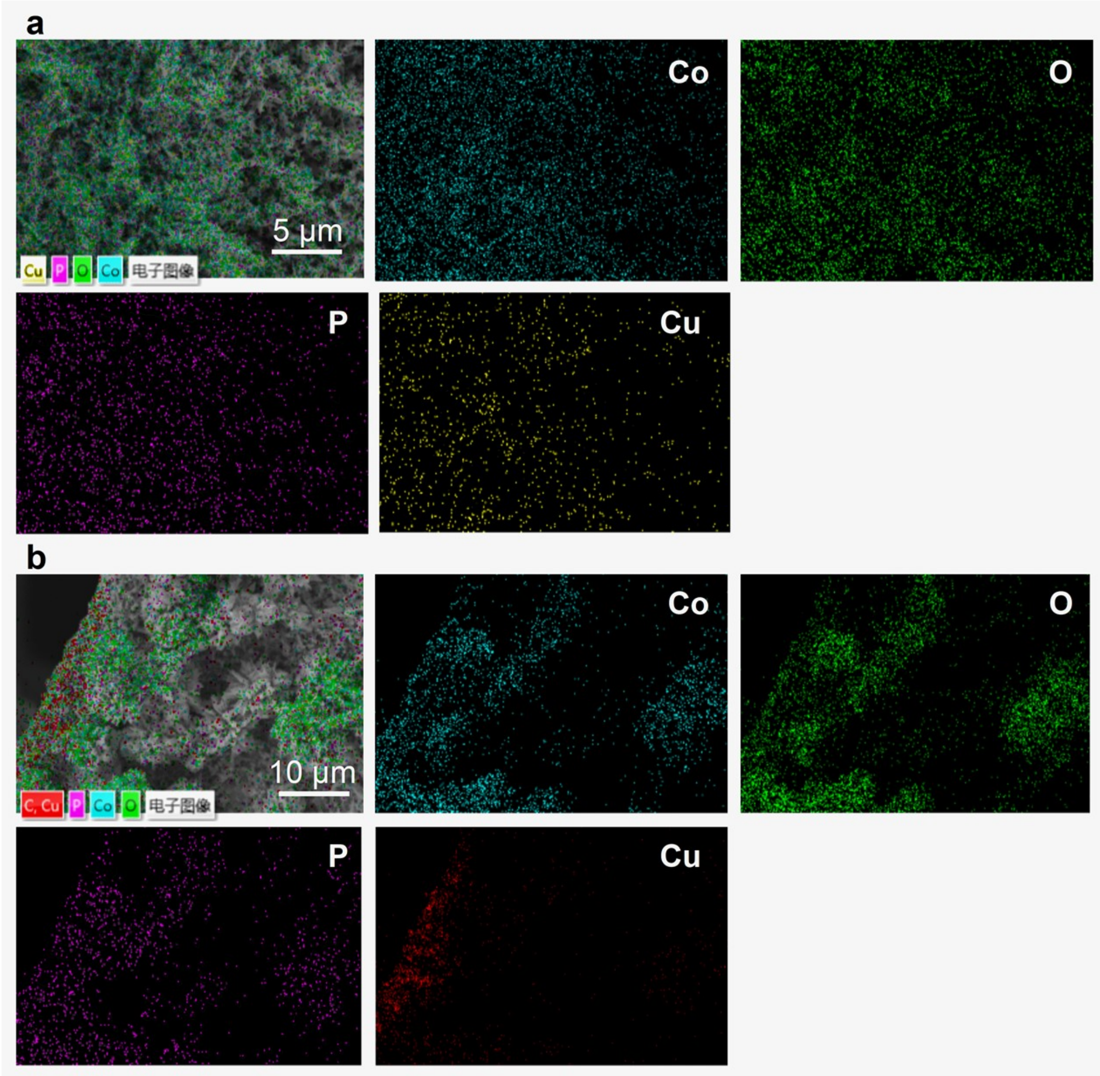

Figure S15. EDS mapping images of anode-side electrode: (a) after OER, (b) after HER of the exchanged sample.

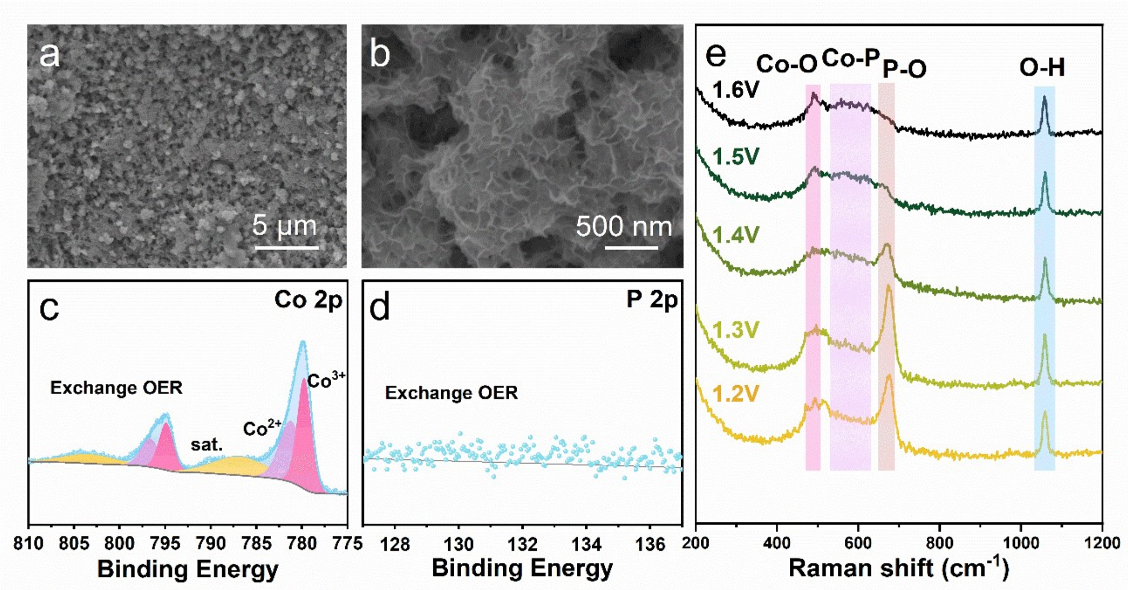

Figure S16. (a-b) SEM and (c-d) XPS maps of the exchanged samples after OER, (e) In-situ Raman diagram of the exchanged samples during OER process.

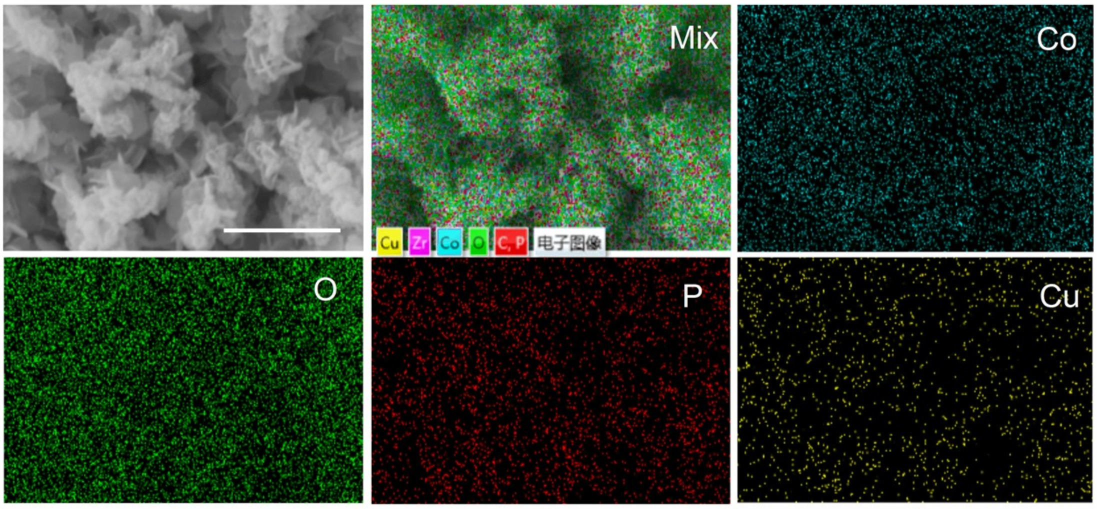

Element	C	O	P	Co	Cu
Atomic%	12.51	56.07	1.79	29.53	0.09

Figure S17. SEM and EDS mapping images of the exchanged sample after OER.

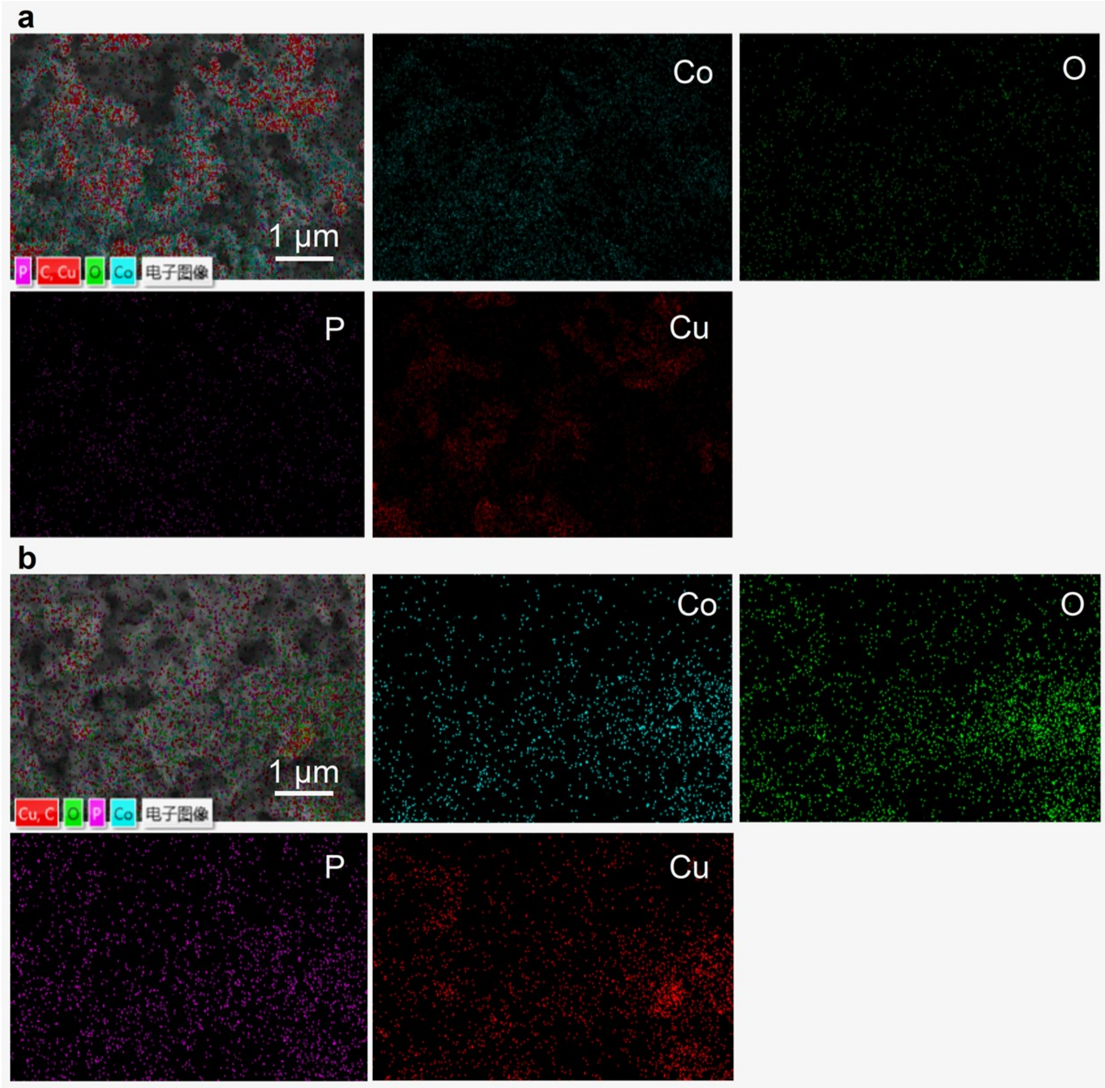

Figure S18. EDS mapping images of cathode-side electrode: (a) after HER, (b) after OER of the exchanged sample.

Table S1 Comparison of different OER electrocatalysts recently reported

Electrocatalyst	**electrolyte**	**Overpotential at 10 mA cm^{-2} (mV)**	**Refs.**
NiCoP-NiS_2/CMT	1M KOH	252	[1]
CoP_2/C	1M KOH	310	[2]
MnV_2O_6/graphene	1M KOH	396	[3]
FeP_2-NiP_2@PC	1M KOH	248	[4]
Co_3O_4-CNTs	1M KOH	370	[5]
FeS_2CL@WS_2NS	1M KOH	280	[6]
PdP_2@CB	1M KOH	270	[7]
NiCoP@rGO	1M KOH	340	[8]
PdCo	1M KOH	310	[9]
NiO-FeO@NiCoO	1M KOH	280	[10]
Fe-Ni_3C-2%	1M KOH	275	[11]
Co_9S_8@NiFe-LDH/NF	1M KOH	287	[12]
CeO_2/C	1M KOH	297	[13]
NCT	1M KOH	331	[14]
$H_2PO_2^-$/FeNi-LDH-V_2C	1M KOH	250	[15]
CoP_2@$Co(CO_3)_{0.5}OH$/Cu/NF	1M KOH	251	this work

Reference

[1] Xue, Y. Wang, H. Zhang, X. Zhao, C. Yao, J. Yan, Q. Zhao, J. Zhu, K. Cao, D. Wang, G. Construction of tubular carbon matrix-supported NiCoP-NiS_2 nanowires with heterointerfaces for overall water splitting. *Colloid. Surface. A* **2023**, 656, 130516.

[2] Dutta, A. Samantara, A. K. Dutta, S. K. Jena, B. K. Pradhan, N. Surface-oxidized dicobalt phosphide nanoneedles as a nonprecious, durable, and efficient OER catalyst. *ACS Energy Lett.* **2016**, 1, 169-174.

[3] Kim, K. H. Choi, Y. H. Hong, S. H. A MnV_2O_6/graphene nanocomposite as an efficient electrocatalyst for the oxygen evolution reaction. *Nanoscale* **2020**, 12, 16028-16033.
[4] Ji, P. Jin, H. Xia, H. Luo, X. Zhu, J. Pu, Z. Mu, S. Double metal diphosphide pair nanocages coupled with P-doped carbon for accelerated oxygen and hydrogen evolution kinetics. *ACS appl. mater. interfaces* **2019**, 12, 727-733.
[5] Shen, J. Gao, J. Ji, L. Chen, X. Wu, C. Three-dimensional interlinked Co_3O_4-CNTs hybrids as novel oxygen electrocatalyst. *Appl. Surf. Sci.* **2019**, 497, 143818.
[6] Zhang, G. Hao, Z. Yin, J. Wang, C. Zhang, J. Zhao, Z. Wei, D. Zhou, H. Li, Z. FeS_2 crystal lattice promotes the nanostructure and enhances the electrocatalytic performance of WS_2 nanosheets for the oxygen evolution reaction. *Dalton T.* **2020**, 49, 9804-9810.
[7] Luo, F. Zhang, Q. Yu, X. Xiao, S. Ling, Y. Hu, H. Guo, L. Yang, Z. Huang, L. Cai, W. Cheng, H. Palladium phosphide as a stable and efficient electrocatalyst for overall water splitting. *Angew. Chem. Int. Edit.* **2018**, 57, 14862-14867.
[8] Mandal, J. R. Singh, K. Shahi, V. K. Amphoteric Membrane Loaded with a Noble Metal-Free Hollow Spherical NiCoP@ rGO Bifunctional Electrocatalyst for Alkaline Water Electrolyzers. *ACS Appl. Energy Mater.* **2022**, 5, 8611-8620.
[9] Kaushik, P. Kaur, G. Chaudhary, G. R. Batra, U. Cleaner way for overall water splitting reaction by using palladium and cobalt based nanocomposites prepared from mixed metallosurfactants. *Appl. Surf. Sci.* **2021**, 556, 149769.
[10] Yan, G. Li, G. Tan, H. Gu, Y. Li, Y. Spinel-type ternary multimetal hybrid oxides with porous hierarchical structure grown on Ni foam as large-current-density water oxidation electrocatalyst. *J. Alloy Compd.* **2020**, 838, 155662.
[11] Fan, H. Yu, H. Zhang, Y. Zheng, Y. Luo, Y. Dai, Z. Li, B. Zong, Y. Yan, Q. Fe-doped Ni_3C nanodots in N-doped carbon nanosheets for efficient hydrogen-evolution and oxygen-evolution electrocatalysis. *Angew. Chem. Int. Edit.* **2017**, 56, 12566-12570.
[12] Gao, X. T. Yu, Z. Zheng, K. X. Yin, J. M. Zheng, Y. Zhu, X. M. Dong, Y. W. Hollow Co_9S_8@NiFe-LDH nanoarrays supported by nickel foam for boosting the

overall water-splitting performance. *Mater. Lett.* **2022**, 319, 132302.
[13] Nazar, N. Manzoor, S. ur Rehman, Y. Bibi, I. Tyagi, D. Chughtai, A. H. Gohar, R. S. Najam-Ul-Haq, M. Imran, M. A. Muhammad, N. Metal-organic framework derived CeO_2/C nanorod arrays directly grown on nickel foam as a highly efficient electrocatalyst for OER. *Fuel* **2022**, 307, 121823.
[14] Ganesan, P. Sivanantham, A. Shanmugam, S. Nanostructured nickel–cobalt–titanium alloy grown on titanium substrate as efficient electrocatalyst for alkaline water electrolysis. *ACS Appl. Mater. Interfaces* **2017**, 9, 12416-12426.
[15] Chen, Y. Yao, H. Kong, F. Tian, H. Meng, G. Wang, S. Mao, X. Cui, X. Hou, X. Shi, J. V_2C MXene synergistically coupling FeNi LDH nanosheets for boosting oxygen evolution reaction. *Appl. Catal. B-Environ.* **2021**, 297, 120474.

Table S2 Comparison of different electrocatalysts recently reported for overall water splitting

Electrocatalyst	electrolyte	Cell voltage	Refs.
$NiCoP-NiS_2/CMT \| NiCoP-NiS_2/CMT$	1M KOH	1.62V, 20 mA cm^{-2}	[1]
$NiCo_2O_4 \| NiCo_2O_4$	1M KOH	1.74V, 20 mA cm^{-2}	[2]
$Ni_3S_2/Ni(OH)_2-NF \| Ni_3S_2/Ni(OH)_2-NF$	1M KOH	1.58V, 20 mA cm^{-2}	[3]
$NiCo_2-N/TiN \| NiCo_2-N/TiN$	1M KOH	1.71V, 20 mA cm^{-2}	[4]
PBSC@FeOOH-20‖PBSC@FeOOH-20	1M KOH	1.638V, 10 mA cm^{-2}	[5]
NiFe-Se/C‖NiFe-Se/C	1M KOH	1.68V, 10 mA cm^{-2}	[6]
$NiFe_2O_4$ @N/rGO‖$NiFe_2O_4$ @N/rGO	1M KOH	1.67V, 20 mA cm^{-2}	[7]
CoP_2@$Co(CO_3)_{0.5}OH/Cu/NF \| CoP_2$@$Co(CO_3)_{0.5}OH/Cu/NF$	1M KOH	1.56V, 20 mA cm^{-2}	[8]
CoP/FeP/CP‖CoP/FeP/CP	1M KOH	1.62V, 10 mA cm^{-2}	[9]
$Pt/Ni_3Fe/rGO \| Pt/Ni_3Fe/rGO$	1M KOH	1.55V, 10 mA cm^{-2}	[10]
$Pt-NiMoO_4-GO/NF \| Pt-NiMoO_4-GO/NF$	1M KOH	1.568V, 10 mA cm^{-2}	this work

Reference

[1] Xue, Y. Wang, H. Zhang, X. Zhao, C. Yao, J. Yan, Q. Zhao, J. Zhu, K. Cao, D. Wang, G. Construction of tubular carbon matrix-supported $NiCoP-NiS_2$ nanowires with heterointerfaces for overall water splitting. *Colloid. Surface. A* **2023**, 656, 130516.

[2] Gao, X. Zhang, H. Li, Q. Yu, X. Hong, Z. Zhang, X. Liang, C. Lin, Z. Hierarchical $NiCo_2O_4$ hollow microcuboids as bifunctional electrocatalysts for overall water-splitting. *Angew. Chem. Int. Edit.* **2016**, 55, 6290-6294.

[3] Wang, H. Wang, C. Zhang, W. Yao, S. A nano-spherical structure $Ni_3S_2/Ni(OH)_2$ electrocatalyst prepared by one-step fast electrodeposition for efficient and durable water splitting. Int. J. Hydrogen Energ. **2022**, 47, 14916-14929.

[4] Tan, C. Wang, F. Lv, K. Shi, Y. Dong, B. Hao, L. Yin, L. Xu, X. Xian, Y. Agathopoulos, S. TiN ceramic membrane supported nitrogen-incorporating $NiCo_2$ nanowires as bifunctional electrode for overall water splitting in alkaline solution. *Sep. Purif. Technol.* **2022**, 298, 121582.

[5] Zhang, Z. He, B. Chen, L. Wang, H. Wang, R. Zhao, L. Gong, Y. Boosting overall water splitting via FeOOH nanoflake-decorated $PrBa_{0.5}Sr_{0.5}Co_2O_{5+\delta}$ nanorods. *ACS Appl. Mater. Interfaces* **2018**, 10, 38032-38041.

[6] Xu, B. Yang, H. Yuan, L. Sun, Y. Chen, Z. Li, C. Direct selenylation of mixed Ni/Fe metal-organic frameworks to NiFe-Se/C nanorods for overall water splitting. *J. Power Sources* **2017**, 366, 193-199.

[7] Cao, L. Li, Z. Su, K. Zhang, M. Cheng, B. Rational design of hollow oxygen deficiency-enriched $NiFe_2O_4$@N/rGO as bifunctional electrocatalysts for overall water splitting. *J. Energy Chem.* **2021**, 54, 595-603.

[8] Zeng L, An L, Zhang Z, et al. Heterogeneous strategy constructing a built-in electric field: CoP/FeP bifunctional electrode for overall water splitting. *Chem Eng J*, **2024**, 491: 152084.

[9] Ni Y, Zhang W, Li Y, et al. Ultralow-content Pt nanodots/Ni 3 Fe nanoparticles: interlayer nanoconfinement synthesis and overall water splitting. *Nanoscale*, **2024**, 16(15): 7626-7633.

[10] Deng X, Chen J, Zhang C, et al. Pt modified NiMoO4-GO/NF nanorods with strong metal-support interaction as efficient bifunctional catalysts for overall water splitting. *J. Colloid Interf. Sci.*, **2023**, 640: 928-939.